Photochemical Electron Transfer in Liquid/Liquid Solvent Systems

Vladimir Mareček,*,† Anna H. De Armond, and M. Keith De Armond*

Contribution from the Chemistry Department, New Mexico State University, Las Cruces, New Mexico 88003. *Received July 7, 1988*

Abstract: A photoinduced charge transfer at the water/1,2-dichloroethane and water/benzonitrile interfaces was studied, using the photoredox couple ruthenium-trisbipyridine complex, $Ru(bpy)_3^{2+}$, dissolved in the organic phase and methyl viologen, MV^{2+}, in the aqueous phase. It was concluded that the photocurrent observed can be ascribed to an electron transfer between the excited ruthenium complex and methyl viologen.

Photochemical charge separation has relevance to a variety of practical problems ranging from the production of H_2 from water splitting to the photosynthetic process itself.[1,2] In both of these general redox schemes, one key to maximizing the overall efficiency of the process is the ability to block the back electron transfer (1a) associated with the photodriven (energy saving) step (1).

$$*D + A \xrightarrow{k_f} D^+ + A^+ \quad (1)$$

$$D^+ + A^- \xrightarrow{k_r} D + A \quad (1a)$$

One strategy for homogeneous media utilizes a sacrificial reagent to react with D^+ or A^- to remove D^+ or A^- rapidly. A classic example of such a system is the $Ru(bpy)_3^{2+}$–MV^{2+} redox couple with EDTA[3] as the sacrificial reagent. An alternative and more effective strategy[4-7] for circumventing the back electron transfer problem uses microscopic interfaces to separate products and reactants spatially on the molecular scale. These microenvironments (molecular assemblies), either charged or neutral, include monolayers, polymer films, microemulsions, micelles, and bilayer lipid membranes.

A simple and unique interface that has generally not been utilized to separate photogenerated reactants and products (block back electron transfer) is the liquid/liquid interface. Such media are valuable as models[8] for the charge transport that occurs in biological membrane systems. Early studies with the water/1,2-dichloroethane (w/dce) solvent system or the water/nitrobenzene (w/nb) system have focused upon ion transfer across the polarized interface.[9,10] A report exists of the $Ru(bpy)_3^{2+}$ and MV^{2+} cation transport across the w/dce and w/nb interfaces.[13] Electron transfer was detected for the $Fe(CN)_6^{3-}/Fe(CN)_6^{4-}$ redox couple in water and ferrocene in nitrobenzene[14] and more recently between $Fe(CN)_6^{3-}$ and lutetium bisphthalocyanine macrocycle.[15]

The present report illustrates photoelectron transport across two different liquid/liquid interfaces using the classic photoredox couple $Ru(bpy)_3^{2+}$–MV^{2+}.

Experimental Section

$Ru(bpy)_3(CBB)_2$ was prepared by precipitation from equimolar aqueous solutions of $Ru(bpy)_3Cl_2 \times 6H_2O$ (Aldrich) and CsCBB (CBB = $(7,8,9,10,11,12\text{-}Br_6\text{-}1\text{-}CB_{11}H_6)^-$ is the hexabromo derivative of monocarborane $(1\text{-}CB_{11}H_{12})^-$—for more details see ref 16). The product was purified by column chromatography on Sephadex LH-20 and recrystallized from acetone. TBACBB (TBA = tetrabutylammonium) was prepared by precipitation from equimolar aqueous solutions of TBAI (Sigma) and CsCBB, followed by several recrystallizations from acetone. The generous gift of TPAsCBB and CsCBB from Dr. K. Baše, Institute of Inorganic Chemistry, Czechoslovak Academy of Sciences, is gratefully acknowledged. LiCl (Fisher), certified grade, and $MVCl_2 \times H_2O$ (Aldrich) were used without further purification. Solutions of $MVCl_2$ and the organic supporting electrolyte were prepared fresh before each measurement. For preparation of aqueous solutions, deionized and distilled water was used. The 1,2-dichloroethane (Aldrich, HPLC grade) was purified by fractional distillation, and only the fraction boiling at 83 °C was used. Benzonitrile (Aldrich) was distilled at reduced pressure, and only the middle fraction with constant boiling point was collected. All organic solvents and photosensitive chemicals were stored in dark bottles wrapped with aluminum foil and kept in the dark.

An all-glass four-electrode cell is shown schematically in Figure 1. The working interface (3) between the aqueous (1) and the organic (2) phase was illuminated from the top of the cell, which was left open. The counter electrode, CE1, was a Cu wire ring, dipped directly into the aqueous solution, while CE2 was separated from the organic phase by sintered glass (5) and immersed in the aqueous solution of LiCl. Reference electrodes, RE1 and RE2 (Ag/AgCl), connected to the working area via Luggin capillaries, were shielded against the light by black PVC tubing (4). The diameter of the working interface was 1.5 cm.

The electrochemical cell, assembled with a battery-operated four-electrode potentiostat equipped with IR compensation,[10] was placed in a Faraday cage. A 200 W high-pressure Hg lamp and optical filters[17] were used for the illumination of the interface. The cut off filters pass light of wavelength longer than 400 nm. A $CuSO_4$ solution was used to filter IR radiation. Photoinduced current was measured by using a lock-in amplifier (SRS Model 530) synchronized with an SRS chopper of frequency 8.4 Hz. The lock-in amplifier was used in the R vector–phase angle mode from which positive values of all ac currents result. Experiments were performed in air-saturated solutions at room temperature, 23 ± 2 °C.

Results and Discussion

Voltammetry at the interface of two immiscible electrolyte solutions (ITIES)—the aqueous and the organic phases—made it possible to follow the transport of charged species (ions and electrons) across the interface. The standard potentials at which

† Visiting professor with current address: J. Heyrovský Institute of Physical Chemistry and Electrochemistry, Czechoslovak Academy of Sciences, Dolejškova 3, 182 23 Prague 8, Czechoslovakia.

(1) Kalyanasundaram, K.; Grätzel, M. *Coord. Chem. Rev.* **1986**, *69*, 57.
(2) Darwent, J. R.; Douglas, P.; Harriman, A.; Porter, D.; Richoux, M. C. *Coord. Chem. Rev.* **1982**, *44*, 83.
(3) Johansen, O.; Mau, A. W. H.; Sasse, W. H. F. *Chem. Phys. Lett.* **1983**, *94*, 113.
(4) Kuhn, H. *Pure Appl. Chem.* **1979**, *51*, 341.
(5) Atik, S. S.; Thomas, J. K. *J. Am. Chem. Soc.* **1981**, *103*, 4367, 7403.
(6) Fendler, J. H. *Acc. Chem. Res.* **1980**, *13*, 7.
(7) Brugger, P. A.; Infelta, P. P.; Braun, A. M.; Grätzel, M. *J. Am. Chem. Soc.* **1981**, *103*, 320.
(8) Koryta, J. *Electrochim. Acta* **1979**, *24*, 293.
(9) Gavach, C. *J. Chim. Phys.* **1973**, *70*, 1478.
(10) Samec, Z.; Mareček, V.; Weber, J. *J. Electroanal. Chem.* **1979**, *100*, 841.
(11) Samec, Z.; Mareček, V.; Weber, J.; Homolka, D. *J. Electroanal. Chem.* **1981**, *126*, 105.
(12) Koryta, J. *Electrochim. Acta* **1984**, *29*, 445.
(13) Samec, Z.; Homolka, D.; Mareček, V.; Kavan, L. *J. Electroanal. Chem.* **1983**, *145*, 213.
(14) Samec, Z.; Mareček, V.; Weber, J.; Homolka, D. *J. Electroanal. Chem.* **1981**, *126*, 105.
(15) Geblewicz, G.; Schiffrin, D. J. *J. Electroanal. Chem.* **1988**, *244*, 27.
(16) Knoth, W. H. *Inorg. Chem.* **1971**, *10*, 598.
(17) Mareček, V.; De Armond, A. H.; De Armond, M. K. *J. Electroanal. Chem.*, in press.

0002-7863/89/1511-2561$01.50/0

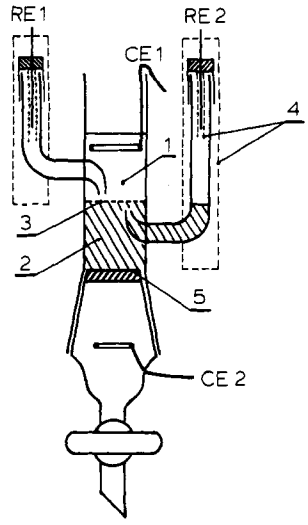

Figure 1. Scheme of the all-glass four-electrode cell: (1) aqueous phase; (2) organic phase; (3) working interface; (4) black PVC tubes for the light protection of the reference electrodes RE1,2; (5) sintered glass, separating counter electrode CE2 from the working space.

the transport of ions occur are proportional to the standard Gibbs free energies of their transfer from water to organic phase $\Delta G_i^{o,Ir\ w\to o}$ (for more details see ref 8 and 12). The absolute value

$$\Delta_o^w\varphi_i^\circ \sim -z_i\Delta G_i^{o,Ir\ w\to o} \qquad (2)$$

of $\Delta G_i^{o,Ir\ w\to o}$ of the base electrolytes have to be higher than those of ions studied to monitor their transport using voltammetry. The values of the free energy of transfer of the base electrolyte ions determine the potential window in which the voltammetry can be done. The potential range available in dce is limited by the transport of ions of organic supporting electrolyte (as follows from our preliminary studies and the published data[18]). Thus, at the positive potentials the transport of $(CBB)^-$ occurs, and, at the negative potentials, the transport of $TPAs^+$ from dce to water occurs. From our preliminary studies in benzonitrile, the potential range available is limited at the positive potentials by the transport of Li^+ from water to benzonitrile and, at the negative potentials, by the transport of $TPAs^+$ from organic phase to water. The positive current is defined as a transparent of cations from water to organic phase and/or of anions from the organic phase to water.[8]

A typical composition of the valvanic cell was

Ag/AgCl	0.01 M LiCl x $MVCl_2$	0.01 M TPAsCBB y $Ru(bpy)_3(CBB)_2$	0.01 M TPAsCl	AgCl/Ag
RE1	(w)	(o)	(w′)	RE2

where x,y vary from zero to 5×10^{-3} M. The cell potential difference E can be written as[10]

$$E = \varphi(w) - \varphi(o) = \Delta_o^w\varphi - \Delta_o^{w'}\varphi^\circ_{TPAs^+} \qquad (3)$$

where $\Delta_o^w\varphi$ is the difference of Galvani potentials across the working interface, and $\Delta_o^{w'}\varphi^\circ_{TPAs^+}$ is the difference of formal potentials of the tetraphenylarsonium ion in both phases.

The transport of MV^{2+} and $Ru(bpy)_3^{2+}$ across the water/1,2-dichloroethane interface is shown in Figure 2. Cyclic voltammograms 1 and 2 (part a) were recorded when 5×10^{-3} M $MVCl_2$ and 5×10^{-3} M $Ru(bpy)_3(CBB)_2$, respectively, were dissolved in the corresponding phases. The increase of the current at the potential of 0.5 V (curve 1(a)) corresponds to the transfer of MV^{2+} from water to organic phase while, at 0.4 V, (curve 2(a)), the

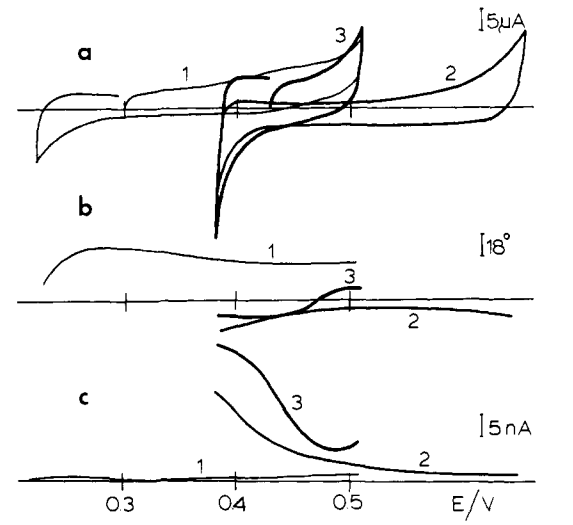

Figure 2. Water/1,2-dichloroethane system (cell I). Part: (a) cyclic voltammograms; (b) dependence of the phase shift of the photoinduced current on the potential; (c) photoinduced current vs potential. Curves: (1) 5×10^{-3} M MV^{2+} (w); (2) 5×10^{-3} M $Ru(bpy)_3^{2+}$ (dce); (3) 5×10^{-3} M MV^{2+} (w) and 5×10^{-3} M $Ru(bpy)_3^{2+}$ (dce).

transfer of $Ru(bpy)_3^{2+}$ from organic phase to water takes place. When both cations are present in the system, the voltammogram 3(a) is recorded. While the illumination of the interface has no effect upon the dc voltammograms, a photoinduced current can be recorded when a more sensitive method is used. In Figure 1 (parts c and b) the ac current amplitude and the phase shift recorded vs potential (using the ac lock-in detection technique) are shown, respectively. Numbering of the curves in parts a, b, and c corresponds to the same composition of the system. While the ac amplitude of the photoinduced current is negligible when only MV^{2+} is present in the system (1c), there is an increase of the ac current below 0.5 V when the $Ru(bpy)_3^{2+}$ is dissolved in the organic phase (2c). This current increase results from the transfer of $Ru(bpy)_3^{2+}$ from the organic phase to water and can be explained by the polarization of the interface by the chopped light.[17] This effect is similar to other electrochemical methods that produce a small perturbation signal. On the other hand, when both redox couples are present, the photoinduced current (curve 3) is most likely caused by the charge-transfer reaction between the luminescent state of $Ru(bpy)_3^{2+}$ and MV^{2+}. Three mechanisms are possible for this reaction, depending upon the microscopic location of the electron-transfer process.

$$^*Ru(bpy)_3^{2+}(o) + MV^{2+}(w) \longrightarrow Ru(bpy)_3^{3+}(o) + MV^{+}(w)$$
$$Ru(bpy)_3^{2+}(o) + MV^{2+}(w) \qquad (4)$$

$$Ru(bpy)_3^{2+}(o) \rightleftharpoons Ru(bpy)_3^{2+}(w) \xrightleftharpoons{h\nu} {}^*Ru(bpy)_3^{2+}(w)$$
$$^*Ru(bpy)_3^{2+}(w) + MV^{2+}(w) \longrightarrow Ru(bpy)_3^{3+}(w) + MV^{+}(w)$$
$$Ru(bpy)_3^{2+}(w) + MV^{2+}(w) \qquad (5)$$

$$MV^{2+}(w) \rightleftharpoons MV^{2+}(o)$$
$$^*Ru(bpy)_3^{2+}(o) + MV^{2+}(o) \longrightarrow Ru(bpy)_3^{3+}(o) + MV^{+}(o)$$
$$Ru(bpy)_3^{2+}(o) + MV^{2+}(o) \qquad (6)$$

The reaction 4 is a photoinduced electron transfer occurring at the interface, while reactions 5 and 6 involve the transfer of $Ru(bpy)_3^{2+}$ or MV^{2+} cations across the interface to the other phase followed by homogeneous electron-transfer reactions. The total photoinduced current will depend on the transfer of reaction products across the interface. Because the photoinduced current increases as the applied potential difference decreases from 0.5 to 0.4 V (cf. 3c, Figure 1), the reaction 6 is not probable, since the concentration of MV^{2+} in the organic phase is decreasing in this potential range. Since the phase shift is decreasing slightly

(18) Koczorovski, Z. *The Interface Structure and Electrochemical Processes at the Boundary between Two Immiscible Liquids*; Kazarinov, V. T., Ed.; Springer Verlag: Berlin, Heidelberg, 1987; p 94.

(19) Wilner and associates have utilized immiscible water/organic systems to facilitate multielectron transfer with 4,4′-bipyridium reductant: *J. Am. Chem. Soc.* **1984**, *106*, 6217.

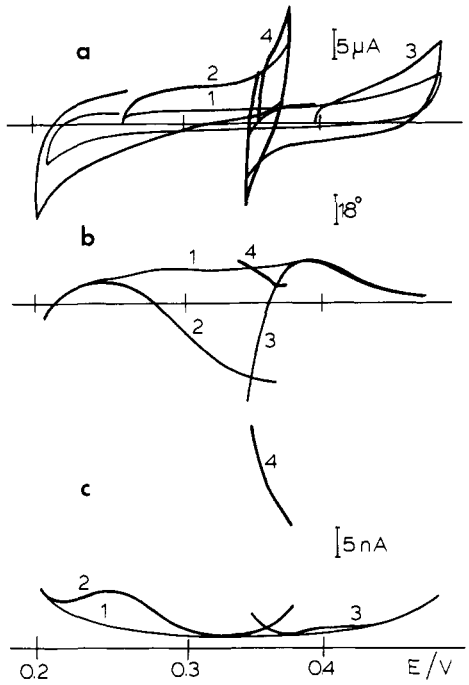

Figure 3. Water/benzonitrile system (cell I). Part: (a) cyclic voltammograms; (b) dependence of the phase shift of the photoinduced current on the potential; (c) photoinduced current vs potential. Curves: (1) base electrolyte system; (2) 5×10^{-3} M MV^{2+} (w); (3) 5×10^{-3} M $Ru(bpy)_3^{2+}$ (bn); (4) 5×10^{-3} M MV^{2+} (w) and 5×10^{-3} M $Ru(bpy)_3^{2+}$ (bn).

when $Ru(bpy)_3^{2+}$ is transferred to the aqueous phase (curve 2, part b) and the opposite effect is observed for the curve 3c at 0.4 V, reaction 5 could be excluded. It can be concluded that the most probable mechanism of the photoinduced charge transfer is that of the reaction 4.

An even larger photoinduced current effect was observed when 1,2-dichloroethane was replaced by benzonitrile (Figure 3). Here the curve 1 corresponds to the base electrolytes and the curve 2 to the addition of 5×10^{-3} M $MVCl_2$ to the organic phase. Due to the higher miscibility of benzonitrile and water, (in comparison with w/dce system), the available potential range when both MV^{2+} and $Ru(bpy)_3^{2+}$ are present (curve 4) is smaller than for the previous case. The observed photoinduced current is higher (curve 4c), and the change of its phase shift is notable, c.f. curve 4 vs 3 and 2 (part b).

The dependence of the photoinduced current on the concentration of $MVCl_2$ is shown in Figure 4, for 10^{-3} M $Ru(bpy)_3^{2+}$ in benzonitrile. Curves 1 and 2 are 10^{-3} M $MVCl_2$ and 10^{-3} M $Ru(bpy)_3^{2+}$, respectively, while the curves 3 were recorded when both were present. The curves 4 are for a solution 5× higher in concentration of $MVCl_2$ than in curves 3.

Finally, in Figure 5 the behavior of the system with benzonitrile, where $TPAs^+$ was replaced by TBA^+, is shown. As was expected, the only difference is a shift of the potential by about 100 mV, which corresponds to the difference of the formal potential differences of TBA^+ and $TPAs^+$ ions. Curve 1 (only in part b) corresponds to the transfer of MV^{2+} (concentrated 5×10^{-3} M), curves 2 (a,b) to 10^{-4} M MV^{2+}, curves 3 to the system with 10^{-3} M $Ru(bpy)_3^{2+}$ and 1.08×10^{-3} M MV^{2+}, and curves 4 were recorded when the concentration of $MVCl_2$ was increased to 1.7×10^{-3} M.

Conclusion

The results reported indicate that the interfaces between water and dce and water and bn can be used to block the back electron transfer[19] between photoexcited $Ru(bpy)_3^{2+}$ and MV^{2+}. No attempt has been made to maximize the efficiency of this process, but degassing of the solvent should enhance it. Also, variation of the hydrophobicity of the excited RuL_3^{2+} complex as well as that of electron acceptor may permit more efficient electron transfer. The use of the w/bn solvent system does give an adequate

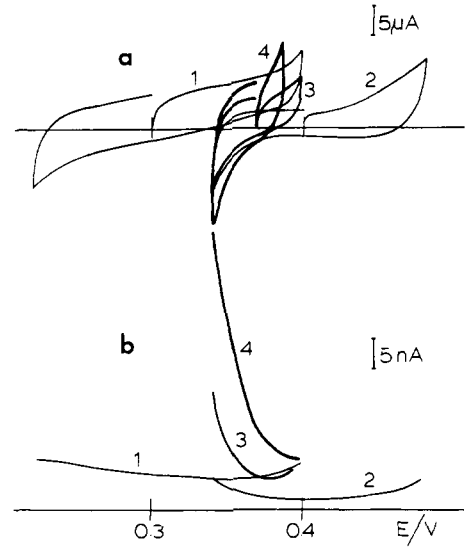

Figure 4. Water/benzonitrile system (cell I). Part: (a) cyclic voltammograms; (b) dependence of the photoinduced current on potential. Curves: (1) 10^{-3} M MV^{2+} (w); (2) 10^{-3} M $Ru(bpy)_3^{2+}$ (bn); (3) 10^{-3} M MV^{2+} (w) and 10^{-3} M $Ru(bpy)_3^{2+}$ (bn); (4) 5×10^{-3} M MV^{2+} (w) and 10^{-3} M $Ru(bpy)_3^{2+}$ (bn).

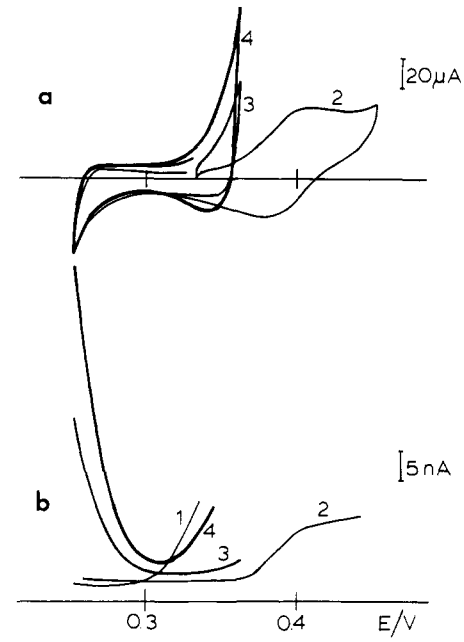

Figure 5. Water/benzonitrile (0.01 M LiCl/0.01 M TBACBB) system. Part: (a) cyclic voltammograms; (b) dependence of the photoinduced current on potential. Curves: (1) 5×10^{-3} M MV^{2+} (w); (2) 10^{-3} M $Ru(bpy)_3^{2+}$ (bn) and 10^{-4} M MV^{2+} (w); (3) 1.08×10^{-3} M MV^{2+} (w) and 10^{-3} M $Ru(bpy)_3^{2+}$ (bn); (4) 1.7×10^{-3} M MV^{2+} (w) and 10^{-3} M $Ru(bpy)_3^{2+}$ (bn).

potential window consistent with variation of the hydrophobicity of the donor and acceptor species. Alternatively, the use of anionic acceptors with cationic metal complex sensitizers may permit a more efficient electron transfer. The possibility of adsorbing an amphiphilic metal complex sensitizer at the interface (in the interface region) may improve the overall electron transfer efficiency if, as suspected, a large fraction of the excited metal complex sensitizers deactivate prior to diffusion to the interface. In any case, the liquid/liquid interface does provide an environment that can be altered by variation of the polarizing species. Such flexibility and ease of preparation should prove advantageous for the general problem of photogenerated charge separation.

In addition, the unique and sensitive photoproperties of RuL_3^{2+} complexes (L = 2,2′-Π-diimine) may permit probing of the double layer structure. For example, the charge-transfer luminescence

of RuL_3^{2+} is sensitive to solvent environment; consequently, the lifetime or emission maxima can, perhaps, in conjunction with laser beam probing of the interface region as a function of polarizing potential, produce some detail concerning the interface structure. In that circumstance where an amphophilic Ru complex can be totally adsorbed at the interface region, the problem of separating bulk from interface Ru complex would be minimized.

Acknowledgment. Support of the Army Research Office (Grant No. 8AAL-03-86-K-0040) is gratefully acknowledged.

Stabilization of Cadmium Selenide Molecular Clusters in Zeolite Y: EXAFS and X-ray Diffraction Studies

Karin Moller,[1a] Mike M. Eddy,[1b] Galen D. Stucky,*[1b] Norman Herron,[1c] and Thomas Bein*[1a]

Contribution from the Department of Chemistry, University of New Mexico, Albuquerque, New Mexico 87131, Department of Chemistry, University of California, Santa Barbara, California 93106, and the Central Research and Development Department,† E. I. du Pont de Nemours & Co., Wilmington, Delaware 19898. *Received July 13, 1988*

Abstract: Small ensembles of CdSe have been synthesized within the cage system of zeolite Y via ion exchange with Cd(II) and subsequent treatment with H_2Se. Cluster size and geometrical arrangements could be determined by comprehensive analysis of Cd- and Se-edge EXAFS data as well as synchroton X-ray powder diffraction and model calculations. The uptake of Se by the zeolite and bond formation to cadmium ions with a bond length of 2.60 Å are clearly evident from EXAFS data of both absorption edges. The CdSe molecular clusters are stabilized at ambient conditions through strong interactions with the zeolite host. Rietveld analysis and EXAFS results indicate the presence of 70% of the cadmium ions at SI′ and 30% at SIII. Se,O-bridged cadmium dimers and Cd_4O_4 cubes are formed in the sodalite unit. Cadmium ions present in 12-ring windows are coordinated to one Se and additional oxygen atoms. Small amounts of Se helical chains and CdSe clusters are also detected.

Semiconductor particles are known to change their electronic, optical, and photochemical properties with particle size. Neither bulk nor molecular properties are encountered in the size range between ~10 and 50 Å. Wider electronic band caps and appearance of new, discrete absorption peaks in the electronic spectra of semiconductor "clusters" in this size range have been interpreted as quantum size effects and exciton formation.[2-4] The synthesis of well-defined semiconducting clusters with homogeneous morphology and size distribution is a prerequisite for understanding the physical origin of these effects. Classical preparation methods for these clusters include wet colloidal techniques,[5-9] growth in dielectric glassy matrices,[10] or growth in polymers.[11] Characterization of cluster size and structure is often difficult to accomplish, especially with cluster sizes smaller than about 20 Å. Particle sizes are usually nonuniform, and agglomeration of individual particles often occurs.[12] Thus the effect of particle size on optical and other properties is obscured.

In recent papers we reported an alternative method to stabilize well-defined semiconductor clusters that are much smaller than those typically formed by classical colloidal techniques. Selenium species and cadmium sulfide ensembles were encapsulated in the crystalline pore structure of zeolite matrices.[13,14] In this paper we present a structural study of closely related cadmium selenide clusters stabilized in zeolite Y. These clusters are composed of a few atoms only that strongly interact with the zeolite host such that their bonding must be considered completely distinct from that of the bulk solid and typical semiconductor clusters. The size domain of the intrazeolite CdSe ensembles compares with that of species produced in gas-phase molecular beam studies. However, the interaction with the zeolite allows us to stabilize these CdSe species in condensed phase at ambient conditions. We observed similar stabilization effects with palladium atoms in zeolites X and Y.[15] Colloidal cadmium selenide is of interest for photosensitized electron-transfer reactions utilized for solar energy conversion and photocatalysis.[16-18]

† Contribution No. 4967.

The constraints provided by the rigid, crystalline aluminosilicate framework of a zeolite offer a considerable improvement in size definition over other preparative environments. Zeolites consist of corner-sharing AlO_4 and SiO_4 tetrahedra connected such that well-defined cavities and channels are formed (see Figure 1). Other metal cations can be introduced by ion exchange of the sodium ions present in the original material. The intrazeolite location of these cations is limited to sites close to framework oxygens that can fulfill the coordination requirements of the cation in question, as shown in Figure 1 for zeolite Y. Sodalite subunits are connected via six-ring windows to form the large supercages

(1) (a) University of New Mexico. (b) University of California. (c) Du Pont Co.
(2) Brus, L. *J. Phys. Chem.* **1986**, *90*, 2555.
(3) Nedeljković, J. M.; Nenadović, M. T.; Mićić, O. I.; Nozik, A. J. *J. Phys. Chem.* **1986**, *90*, 12.
(4) Nozik, A. J.; Williams, F.; Nenadović, M. T.; Rahj, T.; Mićić, O. I. *J. Phys. Chem.* **1985**, *89*, 397.
(5) Henglein, A. *Ber. Bunsenges. Phys. Chem.* **1984**, *88*, 969.
(6) Ramsden, J. J.; Webber, S. E.; Grätzel, M. *J. Phys. Chem.* **1985**, *89*, 2740.
(7) Dannhauser, T.; O'Neil, M.; Johansson, K.; Whitten, D.; McLendon, G. *J. Phys. Chem.* **1986**, *90*, 6074.
(8) Tricot, Y.-M.; Fendler, J. H. *J. Phys. Chem.* **1986**, *90*, 3369.
(9) Variano, B. F.; Hwang, D. M.; Sandroff, C. J.; Wiltzius, P.; Jing, T. W.; Ong, N. P. *J. Phys. Chem.* **1987**, *91*, 6455.
(10) Ekimov, A. I.; Efros, AI. L.; Onushchenko, A. A. *Solid State Commun.* **1985**, 921.
(11) Wang, Y.; Mahler, W. *Opt. Commun.* **1987**, *61*, 233.
(12) Chestnoy, N.; Hull, R.; Brus, L. E. *J. Chem. Phys.* **1986**, *85*, 2237.
(13) Parise, J. B.; MacDougall, J. E.; Herron, N.; Farlee, R.; Sleight, A. W.; Wang, Y.; Bein, T.; Moller, K.; Moroney, L. M. *Inorg. Chem.* **1988**, *27*, 221.
(14) Herron, N.; Wang, Y.; Eddy, M. M.; Stucky, G. D.; Moller, K.; Bein, T.; Cox, D. E. *J. Am. Chem. Soc.* **1989**, *111*, 530.
(15) Moller, K.; Koningsberger, D. C.; Bein, T. *J. Phys. Chem.*, submitted.
(16) Bard, A. J. *J. Phys. Chem.* **1982**, *86*, 172.
(17) Grätzel, M. *Acc. Chem. Res.* **1982**, *15*, 376.
(18) Darwent, J. R. *J. Chem. Soc., Faraday Trans. 1* **1984**, *80*, 183.

0002-7863/89/1511-2564$01.50/0